Available online at www.sciencedirect.com
SCIENCE DIRECT®
Journal of Solid State Chemistry 178 (2005) 3615–3623
JOURNAL OF SOLID STATE CHEMISTRY
www.elsevier.com/locate/jssc

Structure, magnetism and transport of the perovskite manganites $Ln_{0.5}Ca_{0.5}MnO_3$ (Ln = Ho, Er, Tm, Yb and Lu)

Kenji Yoshii[a,*], Hideki Abe[b], Naoshi Ikeda[c]

[a]*Japan Atomic Energy Research Institute, Mikazuki, Hyogo 679-5148, Japan*
[b]*National Institute for Materials Science, Tsukuba, Ibaraki 305-0047, Japan*
[c]*Japan Synchrotron Radiation Research Institute, Mikazuki, Hyogo 679-5198, Japan*

Received 31 May 2005; received in revised form 29 August 2005; accepted 31 August 2005
Available online 27 October 2005

Abstract

It was found that the manganese perovskite oxides $Ln_{0.5}Ca_{0.5}MnO_3$ (Ln = Ho, Er, Tm, Yb and Lu) have an orthorhombic structure (space group *Pnma*). The Mn–O–Mn angles were calculated to be ~148–150°, revealing an existence of a large crystallographic distortion in these oxides. Electrical resistivity measurements indicated both an insulating nature and a small magnetoresistance effect, both of which are owing to narrow bandwidths of the Mn-3*d* electrons arising from the crystallographic distortion. DC magnetization measurements showed the three characteristic temperatures, which could be assigned to charge-order, antiferromagnetism of Mn moments, and possible glassy states. All of these temperatures were decreased for the heavier Ln ions, which is explained in connection with both a difference of ionic radii of Ln^{3+} and Ca^{2+}, and a lowering of electron transfer. The charge-ordering transition was not clearly observed only for $Lu_{0.5}Ca_{0.5}MnO_3$ containing the smallest lanthanide ion, plausibly due to a large randomness of magnetic interactions arising from the ionic radii difference of Lu^{3+} and Ca^{2+}. In addition, preliminary measurements of AC dielectric response suggested that these manganites belong to a so-called multiferroic system.
© 2005 Elsevier Inc. All rights reserved.

Keywords: Perovskite; Manganite; Charge order; Antiferromagnetism; Magnetoresistance

1. Introduction

Manganese oxides $LnMnO_3$ (Ln: lanthanides) have an orthorhombic perovskite structure (space group *Pnma*) for Ln = La–Dy [1–2]. The structure changes to a hexagonal $P6_3cm$ structure for the heavier lanthanides of Ln = Ho–Lu as well as Ln = Y and Sc, all of which contain a two-dimensional (2D) triangular Mn–O lattice [3–9]. These compounds exhibit antiferromagnetic transitions at Néel temperatures (T_N) of ~70–130 K, due to strong antiferromagnetic couplings between the Mn^{3+} moments. Several years ago we reported the magnetic properties of $LnMnO_3$ with Ln = Ho, Er, Tm, Yb and Lu [9]. While the antiferromagnetic transition was observed for the nonmagnetic lanthanide of $Ln^{3+} = Lu^{3+}$, such behavior was not clear for the magnetic lanthanides of $Ln^{3+} = Ho^{3+}$, Er^{3+}, Tm^{3+}, and Yb^{3+}, because of both the large paramagnetic moments of Ln^{3+} and the strong antiferromagnetic interactions between the Mn ions. Recent studies of these manganites have revealed their intriguing physical property, i.e., the coexistence of magnetic order and electric polarization [10]: the oxides are classified into a so-called multiferroic system, the physical properties of which are being attracting much attention in the fields of both fundamental and applied science, because of the potentiality for a fabrication of novel ferroelectric devices [10]. Therefore it is interesting to investigate magnetic and electronic properties of these hexagonal manganites and their derivative systems.

Among possible derivatives of the $LnMnO_3$ oxides, calcium-substituted systems $Ln_{0.5}Ca_{0.5}MnO_3$ (Ln = Ho, Er, Tm, Yb and Lu) were prepared and a few of their magnetic behavior were also briefly commented in Ref. [9]. Magnetic and transport properties of these alkaline-earth-substituted manganites have been studied very extensively

*Corresponding author. Fax: +81 791 58 2740.
E-mail address: yoshiike@spring8.or.jp (K. Yoshii).

0022-4596/$ - see front matter © 2005 Elsevier Inc. All rights reserved.
doi:10.1016/j.jssc.2005.08.033

in this decade [11], since the substitution for lanthanide ions leads to a wide variety of intriguing physical properties such as colossal magneroresistance, metal–insulator transition and charge order. The compounds containing 50% lanthanides, $Ln_{0.5}A_{0.5}MnO_3$ (Ln = lanthanides, A = alkali-earths, $Mn^{3..5+}$), are one of the systems most extensively studied as a representative system among valence-controlled manganites [11–21]. In our paper [9], it was found that $Ln_{0.5}Ca_{0.5}MnO_3$ has an orthorhombic perovskite structure (*Pnma*) and exhibits the anomaly of magnetization was observed between ~220 and ~280 K, which was attributed to charge order of the Mn-3*d* electrons [9].

It is widely known that physical properties of perovskite systems strongly depend on the tolerance factor [11,14], which is determined by the averaged radius of each ion. Roughly, the systems with large average radii of Ln^{3+} and A^{2+} ions, such as $La_{0.5}Sr_{0.5}MnO_3$ [11,22], are ferromagnetic metals owing to large band widths arising from weak lattice distortion. Electrical conductivity is decreased for the compounds containing smaller average radii of Ln^{3+} and A^{2+}. For example, $Pr_{0.5}Ca_{0.5}MnO_3$ becomes an insulating material below ~250 K, accompanied by charge order [11,23]. The properties are governed also by a difference of the ionic radii of Ln^{3+} and A^{2+} [17,24]. From the study of Ln = Gd, Dy, Ho and Er, $Ln_{0.5}Sr_{0.5}MnO_3$ exhibit spin-glass behavior around 40–50 K, while charge order is observed around 250–300 K in the corresponding Ca-substituted oxides $Ln_{0.5}Ca_{0.5}MnO_3$ [17]. This result was interpreted in terms of possible random distribution of magnetic interactions between the Mn ions, which is possibly rooted in the larger difference of ionic radii of Ln^{3+} and A^{2+} in $Ln_{0.5}Sr_{0.5}MnO_3$ than in $Ln_{0.5}Ca_{0.5}MnO_3$. So far, detailed physical properties of the compounds containing the heavier lanthanides of Tm–Lu have been scarcely reported [25]. In this paper, we report detailed investigations on structural, magnetic and transport properties of $Ln_{0.5}Ca_{0.5}MnO_3$ with Ln = Ho–Lu.

2. Experimental procedures

The samples were prepared by a solid-state reaction in air. Stoichiometric mixtures of Ln_2O_3 (Ln = Ho, Er, Tm, Yb and Lu), $CaCO_3$ and Mn_2O_3 (99.9–99.99%, Soekawa) were thoroughly ground, pressed into pellets and fired in air at 1300–1350 °C for 24 h. The firing was repeated for two to three times with intermediate grindings. Each compound was prepared twice in a separate run, and was confirmed to show reproducible structural and magnetic properties. Actual oxygen contents y were 2.96–2.97(2) for $Ln_{0.5}Ca_{0.5}MnO_y$ [9], and showed no apparent trend with changing Ln. For convenience, the compounds will be denoted as $Ln_{0.5}Ca_{0.5}MnO_3$ hereafter. Their crystal structures were determined by powder X-ray diffraction (XRD) using Cu$K\alpha$ radiation between $2\theta = 10^\circ$ and 120° with an angle step of 0.04°. The XRD patterns were refined by the Rietveld method using the program RIETAN-2000 [26]. Magnetic properties were measured using a SQUID magnetometer (Quantum Design MPMS) between 4.5 and 400 K. DC magnetization–temperature (M–T) curves were measured in both field-cooled (FC) and zero-field-cooled (ZFC) modes with the applied fields (H) of 10–1000 Oe. Isothermal magnetization was measured within the applied fields of ±50,000 Oe. AC susceptibilities were measured on heating the samples after zero-field cooling to 4.5 K in the same apparatus with the AC field of 4 Oe. The frequency of the AC field was changed between 0.8 and 1000 Hz. Electrical resistivity was measured by the four prove DC method below 350 K in applied fields of 0 and 7 T.

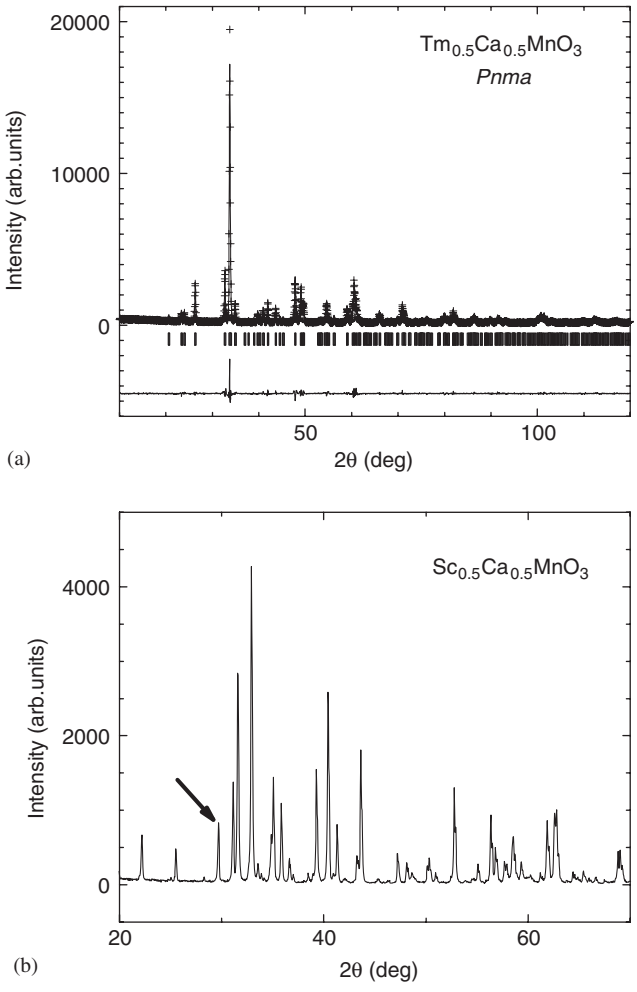

Fig. 1. (a) XRD patterns of $Tm_{0.5}Ca_{0.5}MnO_3$ (space group *Pnma*, $R_{WP} = 8.62\%$, $R_P = 6.60\%$, $R_e = 5.26\%$, $R_F = 1.28\%$). The lattice parameters are $a = 5.4698(5)$, $b = 7.4157(7)$, and $c = 5.2830(5)$ Å. The cross markers and the upper solid line stand for the experimental and fitted patterns, respectively. The vertical markers represent the calculated Bragg angles. The lower solid line shows the difference between the experimental and calculated intensities. The fitting parameters such as atomic positions are listed in Table 1 and are comparable to those reported for other manganites [14]. (b) XRD pattern of "$Sc_{0.5}Ca_{0.5}MnO_3$" obtained by the firing of Sc_2O_3, $CaCO_3$ and Mn_2O_3 at 1350 °C for 24 h. The arrow points out a diffraction peak of Sc_2O_3.

Table 1
Lattice parameters, fractional coordinates, and isotropic thermal parameters of each atom for orthorhombic $Tm_{0.5}Ca_{0.5}MnO_3$ obtained from the Rietveld analysis

Orthorhombic $Tm_{0.5}Ca_{0.5}MnO_3$				
Space group *Pnma*				
$a = 5.4698(5)$, $b = 7.4157(7)$, $c = 5.2830(5)$ Å				
Atom	x	y	z	B (Å^2)
Tm/Ca	−0.0596(2)	0.25	0.9859(4)	0.30(4)
Mn	0.5	0	0	0.23(5)
O(1)	0.5270(15)	0.25	0.0913(18)	0.41(10)
O(2)	0.2007(14)	0.0428(9)	0.7985(15)	0.59(13)

3. Results and discussion

Fig. 1a shows the XRD patterns of $Tm_{0.5}Ca_{0.5}MnO_3$. The experimental pattern could be fitted to the orthorhombic space group of *Pnma*, where Tm and Ca are randomly settled at the same crystallographic site. This structure is identical to those reported for some other $Ln_{0.5}A_{0.5}MnO_3$ oxides (A = Ca and Sr) with the larger Ln^{3+} ions (such as Sm^{3+}) [11–22]. Some fitting parameters are listed in Table 1, where the definition of fractional coordinates of each atom was aligned with that for an isostructural $Ho_{0.5}Sr_{0.5}MnO_3$ [15]. It is relevant that all the coordinates are comparable to those for $Ho_{0.5}Sr_{0.5}MnO_3$. The fit based on the same crystal structure of *Pnma* could be carried out also for the other $Ln_{0.5}Ca_{0.5}MnO_3$ oxides. We have also attempted the synthesis of $Sc_{0.5}Ca_{0.5}MnO_3$, which contains a smaller trivalent ion of Sc^{3+} than Lu^{3+}. The XRD pattern in Fig. 1b shows a presence of the starting material of Sc_2O_3 and has not been successfully fitted for any single-phase compounds.

The obtained lattice parameters plotted in Fig. 2a show that all the parameters seem to change almost continuously. The monotonic decrease in the cell volume was confirmed by the present data and is in accord with the lanthanide contraction. The calculated Mn–O–Mn angles from the obtained parameters were found to be quite small of ~148–150°, which indicates a large lattice distortion brought about by the small ionic radii of Ln^{3+} (1.072–1.032 Å) and Ca^{2+} (1.18 Å) [27]. The average Mn–O–Mn angle for each oxide was plotted in Fig. 2b. The angle becomes narrowed for the heavier *Ln* ions, which indicates an enhancement of lattice distortion arising from the lanthanide contraction.

In the figure, the tolerance factor (t) and the variance of the Ln^{3+} and Ca^{2+} ions (σ^2) are shown as well. The former value is defined as $t = (r_A + r_O)/\sqrt{2}(r_{Mn} + r_O)$, where r_A, r_O, r_{Mn} stand for the average radius of Ln^{3+} and Ca^{2+}, the radius of the O^{2-} ion, and the average ionic radius of Mn^{3+} and Mn^{4+}, respectively. This value is a measure of lattice distortion as has been widely known from many studies of perovskites: Lattice distortion is enhanced for smaller t values. On the other hand, the latter value defined as $\sigma^2 = \sum y_i r_i^2 - r_A^2$ could be regarded as a measure of local structural disorder, corresponding to a random distribution of Mn–O–Mn bond angle [28,29]. Here, y_i, r_i^2 and r_A means the contents of Ln^{3+} and Ca^{2+} (i.e., $y_i = 0.5$), ionic radius of either Ln^{3+} or Ca^{2+}, and the average ionic radius of Ln^{3+} and Ca^2. This value is governed by the difference of the ionic radii of Ln^{3+} and Ca^{2+}, as well as the absolute value of each ionic radius. It is expected that the disorder becomes more intensified with increasing σ^2.

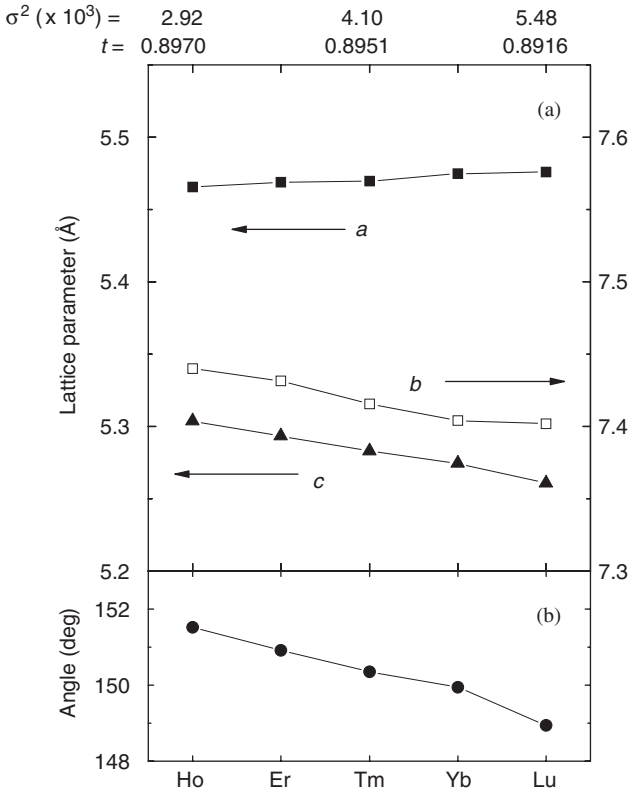

Fig. 2. (a) Lattice parameters and (b) Average Mn–O–Mn angles plotted for all the compounds, which are expressed in terms of the *Ln* atom in $Ln_{0.5}Ca_{0.5}MnO_3$ (*Ln*: lanthanides). The t and σ^2 values are shown as well, whose details are noted in the text.

From these discussion on the tolerance factor, the results in Fig. 1b strongly suggests that the $Sc_{0.5}Ca_{0.5}MnO_3$ phase is unstable at an ambient pressure plausibly owing to a large lattice distortion. The synthesis of the corresponding Sr-compounds, $Ln_{0.5}Sr_{0.5}MnO_3$ with Ln = Ho–Lu, and Sc, was also attempted. It was found that single-phase samples could be prepared only for $Ho_{0.5}Sr_{0.5}MnO_3$ as was reported [15]. On the assumption of the *Pnma* structure also for these oxides, the tolerance factors of $Ln_{0.5}Sr_{0.5}MnO_3$ are calculated to be larger than ~0.915 for Ln = Ho–Lu. As this value is larger than those of the corresponding Ca-compounds (Fig. 2), it is plausible that lattice distortion is not an origin of the instability of the Sr-system. The same *Pnma* structure for $Ln_{0.5}Sr_{0.5}MnO_3$ provides larger values of σ^2 ($\gtrsim 1.42 \times 10^{-2}$) than for the Ca-system (Fig. 2). Therefore, it is inferred that the instability of $Ln_{0.5}Sr_{0.5}MnO_3$ with Ln = Er–Lu, and Sc is

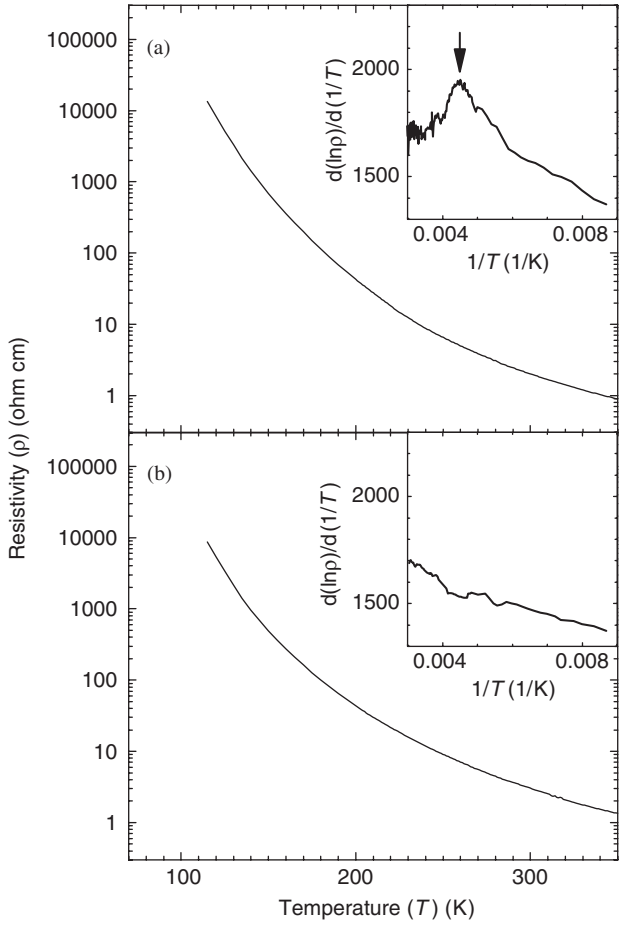

Fig. 3. Electrical resistivity (ρ) plotted against temperature (T) for (a) $Yb_{0.5}Ca_{0.5}MnO_3$ and (b) $Lu_{0.5}Ca_{0.5}MnO_3$. The insets shows the derivative values of $d(\ln\rho)d(1/T)$ to determine the charge-ordering temperature (T_{CO}). The peak temperature pointed by the arrow for $Yb_{0.5}Ca_{0.5}MnO_3$ corresponds to T_{CO}~220 K.

ascribable to large local disorder at the crystallographic A-site.

Fig. 3a and b show the electrical resisitivity (ρ) plotted against temperature (T) for $Ln_{0.5}Ca_{0.5}MnO_3$ with Ln = Yb and Lu, respectively. All the $Ln_{0.5}Ca_{0.5}MnO_3$ oxides were found to be insulating below 350 K. This behavior originates from a small electron transfer of the Mn-3d electrons, because of the small Mn–O–Mn angles. For the present $Ln_{0.5}Ca_{0.5}MnO_3$ oxides with Ln = Ho and Er, charge-ordering transitions of the Mn-3d electrons were suggested at T_{CO}~280 and ~260 K, respectively, where a slight change of temperature dependence of resistivity appeared as in the previous paper [17]. In this work, $Ln_{0.5}Ca_{0.5}MnO_3$ also with Ln = Tm and Yb also exhibited such a change at ~250 and ~220 K, respectively. The charge-ordering phenomenon has been often reported for manganites with small tolerance factors (t) and has been understood in connection with the localizability of the Mn-3d electrons, arising from small Mn–O–Mn angles. Because the change of temperature dependence of resisitivity was very slight for Ln = Tm and Yb, derivative of logarithm of resistivity ($\ln\rho$) was taken against inverse temperature ($1/T$) to estimate the charge-ordering temperature T_{CO} [19]. The result for Ln = Yb is shown in the inset of Fig. 3a. As is the case of an isostructural $Y_{0.5}Ca_{0.5}MnO_3$ with T_{CO} of 260 K [19], a maximum of the derivative is noticed. The derivative exhibits its peak at $1/T$~0.0045, which corresponds to T~220 K. This temperature is denoted as T_{CO} and is close to that calculated from the temperature derivative of inverse magnetization shown later. From the present data, the activation energies at 350 and 200 K were estimated to be 0.13 and 0.16 eV, respectively. It is noteworthy that T_{CO} is decreased from ~280 to ~220 K with increasing the atomic number of Ln from Ho to Yb (see Fig. 9 for brevity). For $Lu_{0.5}Ca_{0.5}MnO_3$ containing the smallest Ln^{3+} ion, no clear maximum or minimum was obtained in the temperature derivative curves, as is shown in the inset of Fig. 3b. Therefore, charge order is suppressed in this compound. Magnetoresistance measurements with the field of 70,000 Oe (7 T) were also carried out and showed a small decrease in resistivity (by ~20% at the largest) below T_{CO} for Ln = Tm, Yb, and Lu. The magnetoresistance for Ln = Ho and Er is roughly an order of 100% [16]. The result for $Lu_{0.5}Ca_{0.5}MnO_3$ is shown in Fig. 4. The small magnetoresistance effect is an analogous property to those reported for the manganites having small tolerance factors, such as $Y_{0.5}Ca_{0.5}MnO_3$ (t = 0.8992) [19] and $Ho_{0.5}Sr_{0.5}MnO_3$ (t = 0.9218) [15]. The result is qualitatively explained in connection with weak ferromagnetic couplings between the Mn-e_g electrons, brought about by the large lattice distortion [15].

Fig. 5a and b shows the M–T curves measured with H = 1000 Oe in the FC mode for $Ln_{0.5}Ca_{0.5}MnO_3$ with Ln = Ho, Er, Tm, and Yb. For these oxides where the Ln^{3+} ions have the localized 4f moments, both of the FC and ZFC curves exhibits a monotonic increase in magnetization at low temperatures. This is because of a paramagnetic response of the Ln^{3+} moments, as was proposed for $LnMnO_3$ [9]. The curves for Ln = Ho and Er

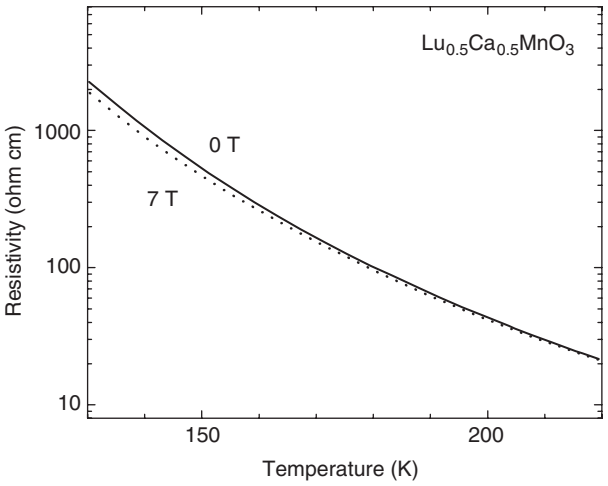

Fig. 4. Magnetoresistance of $Lu_{0.5}Ca_{0.5}MnO_3$ measured under 0 T (solid line) and 7 T (dotted line).

exhibited a change of temperature dependence of magnetization around 280 and 260 K, respectively, which is shown only for $Ln = Ho$ in the inset. Judging from the present resistivity data as well as the literature data [17], this change is owing to the charge-ordering transition of the Mn-3*d* electrons. The change is not clear in the magnetization curves for $Ln = Tm$, Yb and Lu. The result for $Ln = Tm$ and Yb is shown in Fig. 5b, indicating that the charge order is more suppressed for the heavier lanthanides in the $Ln_{0.5}Ca_{0.5}MnO_3$ series.

The measurements with the low applied magnetic fields of 10–20 Oe for $Ln = Ho$ and Er (Ref. [17]) provided a deviation between the FC and ZFC curves, which elucidates a presence of magnetic irreversibility. This is shown in the inset of Fig. 5b for $Ln = Tm$. The deviation temperature of ~90–100 K could be defined as the magnetic transition temperature. However, determination of such a temperature is difficult because of very slight difference of magnetization near the transition. In this work, the transition temperature was determined from temperature derivative of inverse magnetization.

Inverse magnetization ($1/M$) was plotted against temperature (T) for $Tm_{0.5}Ca_{0.5}MnO_3$ in Fig. 5c. As is the case of isostructural $Tb_{0.5}Ca_{0.5}MnO_3$ (Ref. [16]) and $Y_{0.5}Ca_{0.5}MnO_3$ [19], one can see the three characteristic temperatures, each of which was defined from the temperature derivative of this curve shown in the inset. The highest temperature of ~250 K is regarded as the charge-ordering temperature (T_{CO}), because this

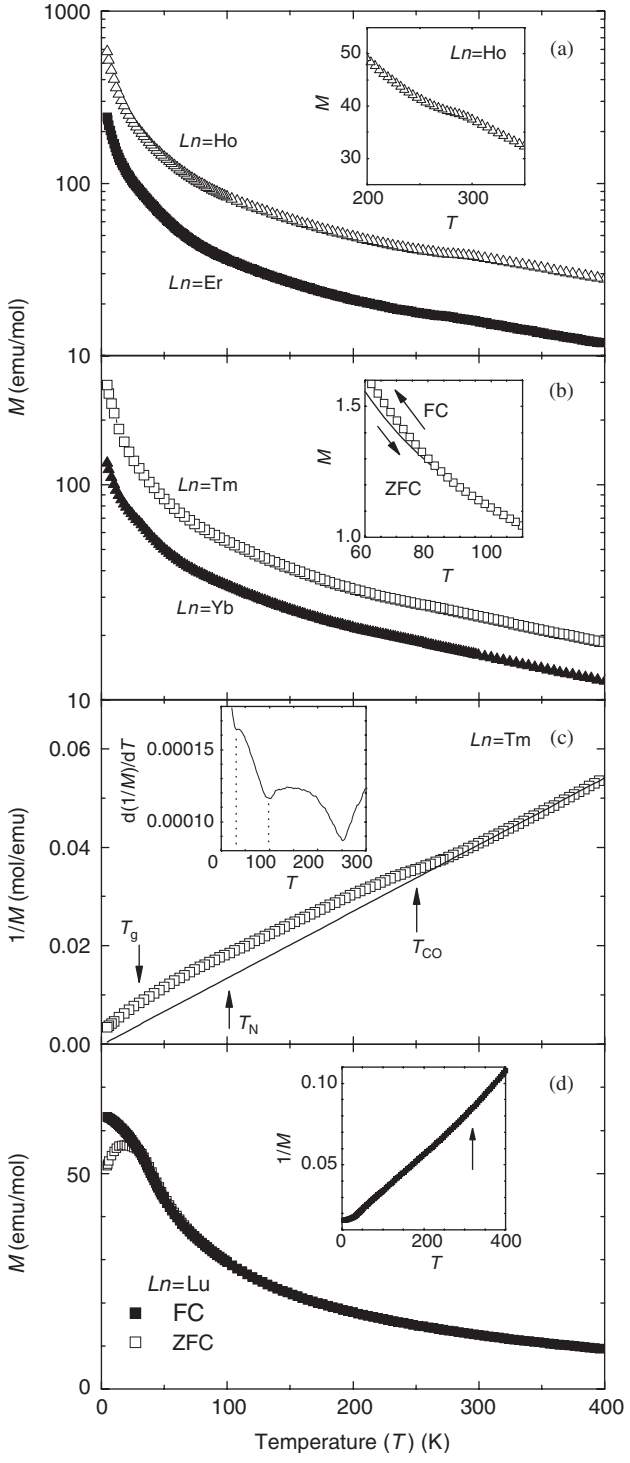

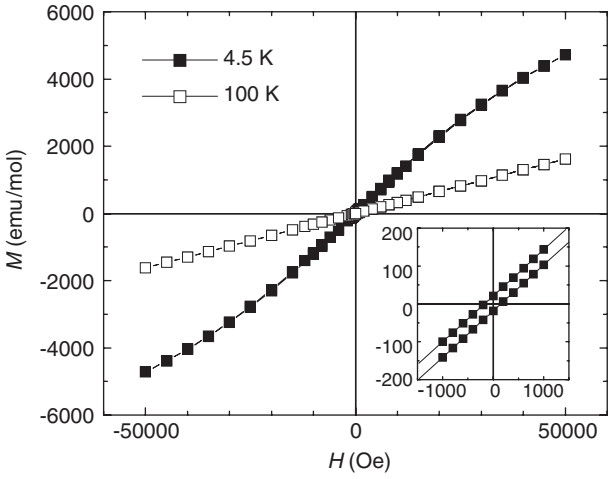

Fig. 6. Isothermal magnetization (M) at 4.5 and 100 K plotted against applied field (H) for $Yb_{0.5}Ca_{0.5}MnO_3$ (T_N~90 K) The inset shows a low applied-field region of the data at 4.5 K.

Fig. 5. Magnetization–temperature (M–T) curves for $Ln_{0.5}Ca_{0.5}MnO_3$ with $Ln = Ho$, Er, Tm, Yb, and Lu. Each oxide is expressed in terms of the Ln atom: (a) field-cooled (FC) M–T curves for $Ho_{0.5}Ca_{0.5}MnO_3$ and $Er_{0.5}Ca_{0.5}MnO_3$ measured with an applied field (H) of 1000 Oe. The inset shows the temperature region around T_{CO} (~280 K). (b) FC M–T curves for $Tm_{0.5}Ca_{0.5}MnO_3$ and $Yb_{0.5}Ca_{0.5}MnO_3$ measured with $H = 1000$ Oe The inset shows the FC (open squares) and zero-field-cooled (ZFC; solid line) curves around T_N (~102 K) for $Tm_{0.5}Ca_{0.5}MnO_3$ measured with $H = 20$ Oe. (c) Inverse magnetization ($1/M$) plotted against temperature for $Tm_{0.5}Ca_{0.5}MnO_3$. The open squares and the solid line represent the experimental data and the Curie–Weiss fit, respectively. The inset shows the temperature derivative of $1/M$ to estimate the value of T_{CO} T_N and T_g (pointed by the arrows). (d) M–T curves for $Lu_{0.5}Ca_{0.5}MnO_3$ measured with $H = 1000$ Oe. The inset shows the inverse magnetization data, where the arrow points out the deviation temperature from the Curie–Weiss law. Further details are noted in the text.

temperature was well close to that obtained from the resistivity data. The Weiss temperature above T_{CO} was calculated as a weakly ferromagnetic value of ~1 K. This temperature is much larger than that for $TmMnO_3$ (~−60 K) [9], where strong antiferromagnetic couplings exist between the Mn^{3+} ions. This difference indicates a presence of ferromagnetic double-exchange interactions in $Tm_{0.5}Ca_{0.5}MnO_3$. In fact, the paramagnetic effective moment above T_{CO} was very close to that calculated by use of the magnetic moments of Mn^3 ($t_{2g}^3e_g^1$; $S=2$; 4.90 μ_B), Mn^{4+} ($t_{2g}^3e_g^0$; $S=3/2$; 3.87 μ_B), and Tm^{3+} ($4f^{12}$; 7.6 μ_B) [30]. This configuration provides a ferromagnetic double-exchange interaction between the Mn^{3+} and Mn^{4+} ions through an electron transfer between the Mn-e_g orbitals

The second characteristic temperature of ~100 K is close to that at which the deviation of FC and ZFC curves occurs (Fig. 5b). Therefore this can be assigned to the magnetic transition temperature. The existence of magnetic order is verified by the isothermal magnetization measurements (Fig. 6 for brevity). If the Curie–Weiss law is applied to the temperature region between ~100 and ~210 K, the Weiss temperature is calculated to be an antiferromagnetic value of −45 K. Thus this transition is regarded as antiferromagnetic order, as was discussed for $Y_{0.5}Ca_{0.5}MnO_3$ [19], $Tb_{0.5}Ca_{0.5}MnO_3$ [16], $Ho_{0.5}Ca_{0.5}MnO_3$ and $Er_{0.5}Ca_{0.5}MnO_3$ [17]. This temperature is denoted as T_N. The paramagnetic effective moment in this temperature region was almost the same as that above T_{CO}. The result shows a coexistence of the paramagnetic Mn^3 ($t_{2g}^3e_g^1$; $S=2$; 4.90 μ_B), Mn^{4+} ($t_{2g}^3e_g^0$; $S=3/2$; 3.87 μ_B) moments also in this region. An origin of the lowest characteristic temperature of ~30 K is likely either a spin-glass or a similar phase denoted as cluster-glass [16], on the basis of the AC susceptibility and the magnetization data for $Lu_{0.5}Ca_{0.5}MnO_3$ shown later. This temperature is denoted as T_g hereafter. It should be noted that all the temperatures T_{CO}, T_N and T_g are decreased monotonically with increasing the atomic number of *Ln*.

Fig. 5d shows the magnetization plotted against temperature for $Lu_{0.5}Ca_{0.5}MnO_3$ where the Lu^{3+} ion is nonmagnetic ($4f^{14}$). It is seen that the deviation of the FC and ZFC curves occurs below ~40 K, which is indicative of magnetic order. The transition temperature was obtained as ~40 K from the temperature derivative of inverse magnetization. Though the Weiss temperature above ~300 K was ferromagnetic of ~45 K, this temperature is tentatively assigned to T_N considering the transition profile, an absence of saturation magnetization (not shown), and the antiferromagnetic Weiss temperatures (between T_N and T_{CO}) for the other $Ln_{0.5}Ca_{0.5}MnO_3$ oxides. The T_g value was estimated as ~20 K, which will be shown from the AC susceptibility data. The inset shows the inverse magnetization plotted against temperature for $Lu_{0.5}Ca_{0.5}MnO_3$. The curve exhibits a slight bending at ~300 K, though no sharp minimum or maximum was obtained in the temperature derivative. The effective paramagnetic moment below ~300 K is considerably larger (by ~40%) than the value of 4.42 μ_B/Mn calculated from the moments of Mn^{3+} ($t_{2g}^3e_g^1$; $S=2$; 4.90 μ_B) and Mn^{4+} ($t_{2g}^3e_g^0$; $S=3/2$; 3.87 μ_B). A possibility of this behavior is a tendency toward either magnetic or charge order. Such a change of slope around 300 K was not clearly found for the other oxides: It is masked by the large paramagnetic response of the Ho^{3+}, Er^{3+}, Tm^{3+}, and Yb^{3+} moments (~4.5–10.6 μ_B) [30].

Fig. 6 shows the isothermal magnetization (M) plotted against the applied field (H) at 4.5 and 100 K for $Yb_{0.5}Ca_{0.5}MnO_3$ (T_N~90 K). The inset represents a magnetic hysteresis accompanied by small remanence of ~20 emu/mol at 4.5 K. The absence of saturation magnetization is in accord with the existence of the antiferromagnetic order. The curve becomes paramagnetic without clear remanence above T_N, which is demonstrated by the data at 100 K.

Fig. 7 shows the real part of AC susceptibility (χ') for $Lu_{0.5}Ca_{0.5}MnO_3$. The two peaks exist at ~20 and ~35 K. Considering the T_N value of ~40 K estimated from the temperature derivative of inverse magnetization, the peaks at the higher temperature of ~35 K is tentatively assigned to that of the antiferromagnetic order. With changing the frequency of the AC field, only the peak at the lower temperature of ~20 K tends to slightly shifts to higher temperatures as pointed by the arrows, while the higher-temperature peak exhibits no apparent shift. As has been well known, such a peak shift is one characteristic for magnetically frustrated system denoted as spin-glass or cluster-glass [31]. The existence of a glassy state is supported by the logarithmic time-dependent change of magnetization at 5 K shown in Fig. 8, which has been reported as one of the typical phenomena of glassy systems [31]. A cluster-glass transition below T_N was proposed for $Tb_{0.5}Ca_{0.5}MnO_3$ (T_{CO}~300 K, T_N~120 K) showing an anomaly in the magnetization curves at ~50 K [16]. The

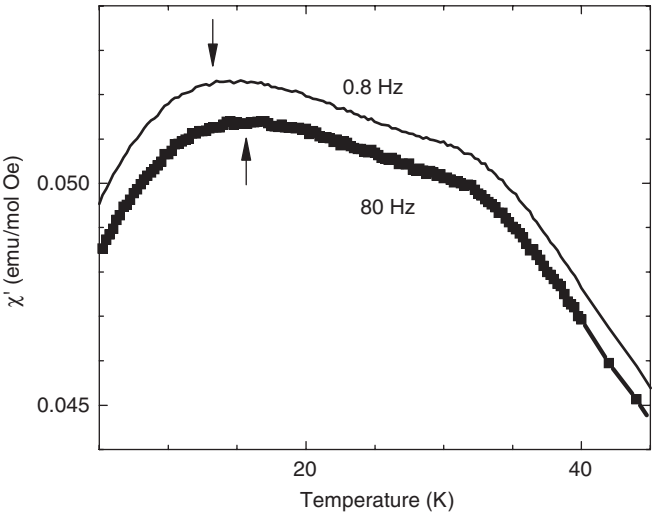

Fig. 7. Real part of AC susceptibility (χ') for $Lu_{0.5}Ca_{0.5}MnO_3$ measured with the AC field of 4 Oe. The frequencies of the AC field are 0.8 and 80 Hz. The susceptibility for 80 Hz was decreased by 5×10^{-4} emu/mol Oe.

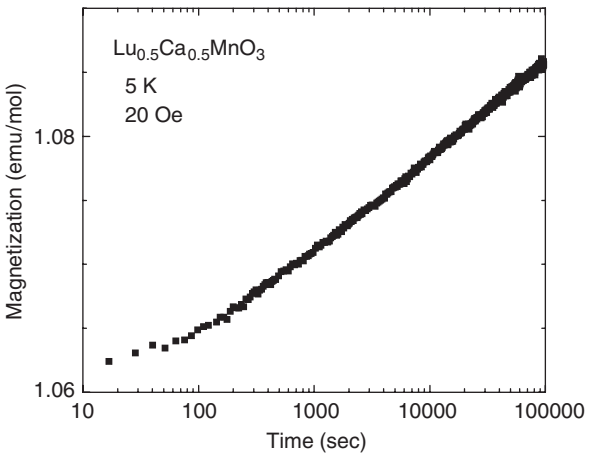

Fig. 8. Magnetization plotted against time evolution at 5 K for $Lu_{0.5}Ca_{0.5}MnO_3$. The sample was zero-field-cooled down to 5 K. Then the measurement was done immediately after the magnetic field of 20 Oe was applied.

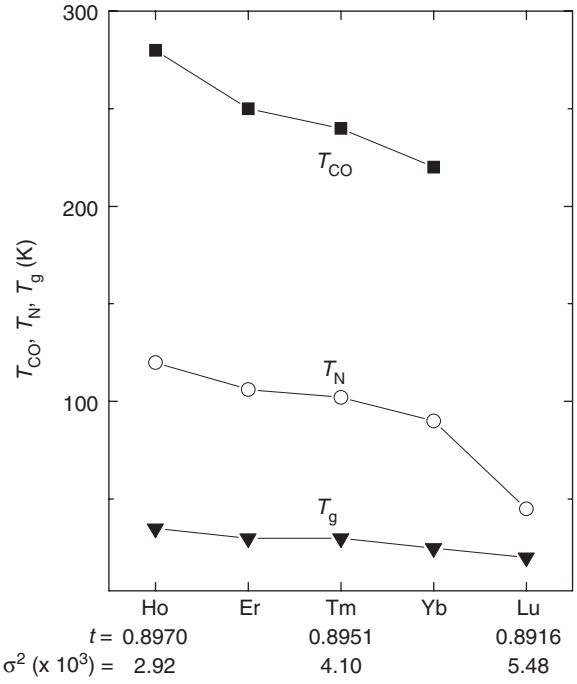

Fig. 9. The values of T_{CO}, T_N, and T_g against the *Ln* ion for all the $Ln_{0.5}Ca_{0.5}MnO_3$ studied (*Ln*: Ho–Lu). The t and σ^2 values are shown as well.

absence of the shift of the higher-temperature peak in Fig. 7 strongly suggests its origin of the antiferromagnetism [31]. Time-dependent magnetization measurement around this temperature as shown in Fig. 8 provided almost a constant magnetization value for 24–48 h. Though the AC susceptibility measurements were carried out for the other $Ln_{0.5}Ca_{0.5}MnO_3$ compounds, their susceptibilities provided similar temperature dependence to those of magnetization curves, because the temperature dependence is governed mainly by the large paramagnetic Ln^{3+} moments [30].

The experimental results obtained from the magnetic measurements are summarized in Fig. 9. It was confirmed that the T_{CO} values determined from the inverse magnetization were almost the same as those from the resistivity data. Though a quantitative explanation of the data requires theoretical calculations, qualitative discussions can be given in the following.

The charge-ordering phase below T_{CO} is favored if the Mn-3*d* electrons tend to be localized, which has been often reported for the manganites having the small tolerance factors (t). Experimentally, the transition from the charge-ordered phase to the antiferromganetic phase also has been reported for some other $Ln_{0.5}Ca_{0.5}MnO_3$ oxides [16,17,19]. The ferromagenetic to antiferromagnetic change of the Weiss temperature at T_{CO} (Fig. 6c) indicates that the charge-ordering transition weakens ferromagnetic double-exchange interactions, because of a narrowing of the Mn-e_g bandwidth. Namely, antiferromagnetic superexchange interactions between the Mn-t_{2g} orbitals are dominant below T_{CO} instead. This change causes the antiferromagnetic order at T_N. It is worth pointing out that the stabilization of antiferromagnetic phase accompanied by charge order was rationalized by the theoretical simulation for the magnanites having narrow bandwidths (like the present compounds) [32]. As is the case of $Ln_{0.5}Sr_{0.5}MnO_3$ (*Ln* = Dy, Gd, Ho and Er) with T_g~40–50 K [17,24], the glassy phase below T_g (~20–30 K) may be ascribed to the random distribution of magnetic interactions, originating from the difference of ionic radii of Ln^{3+} and A^{2+}. The true mechanism for the appearance of this phase should be clarified in future.

Another characteristic feature in Fig. 9 is that all of T_{CO}, T_N and T_g values are monotonically decreased when the atomic number of *Ln* is increased in $Ln_{0.5}Ca_{0.5}MnO_3$: T_{CO} is lowered from ~280 and ~220 K, T_N from ~110 to ~40 K, and T_g from ~35 to ~20 K. The change of T_N and T_g is qualitatively understood in terms of the weakening of magnetic interactions rooted in the enhanced lattice distortion, which manifests itself as the smaller tolerance factors (t) as well as the smaller Mn–O–Mn angles (Fig. 2) for the heavier *Ln* atoms. It is reasonable that T_{CO}~280 K and T_N~110 K for $Ho_{0.5}Ca_{0.5}MnO_3$ are comparable to those for $Y_{0.5}Ca_{0.5}MnO_3$, T_{CO}~260 K and T_N~130 K, as the ionic radius of Y^{3+} (1.075 Å) is very close to that of Ho^{3+} (1.072 Å) [27]. Together with the previous experimental data of other $Ln_{0.5}Ca_{0.5}MnO_3$ oxides (*Ln* = La to Er, and Y), T_{CO} exhibits the maximum of ~310 K for *Ln* = Gd ($t = 0.905$, $\sigma^2 = 1.33 \times 10^{-3}$) [17].

Since it seems that the charge-ordered phase is more favored as the Mn-3*d* electrons tend to be more localized, T_{CO} is expected to increase monotonically with increasing the atomic number of *Ln*. However, the experimental result is not the case. The behavior of T_{CO} for *Ln* = Ho–Lu shown in Fig. 9 is likely interpreted in connection with the increase in σ^2. As the atomic number of *Ln* is increased from La to Lu, the difference of the ionic radii is also increased monotonically. This change is expressed by use

of the σ^2 value: the value increases from 3.24×10^{-4} for $Ln = La$ to 5.48×10^{-3} for $Ln = Lu$. Thus, taking into account the random settlement of Ln^{3+} and Ca^{2+} at the same crystallographic site, spatial randomness of magnetic interactions between the Mn ions is enhanced for the heavier *Ln* ions [17]. This situation makes it difficult to realize long-range phase transitions including charge order. The results in both Fig. 9 and Ref. [17] experimentally shows a crossover between the effects from the localizability favoring the charge order (measured by the t value) and the spatial randomness favoring no order (measured by the σ^2 value) around $Ln = Gd$. Namely, the data for the heavier *Ln* atoms than Gd are understood in terms of the suppression of charge order brought about by the enhancement of randomness. The randomness effect is expected to become the largest for the smallest lanthanide ion of $Ln^{3+} = Lu^{3+}$. Therefore, the absence of T_{CO} in $Lu_{0.5}Ca_{0.5}MnO_3$ means that such an effect is large enough to constrict a charge-ordering transition in this system.

To reveal more details of the physical properties in the present system, measurements of AC dielectric response were carried out for a few samples [33]. The result for $Lu_{0.5}Ca_{0.5}MnO_3$ is shown in Fig. 10. The large dielectric constants of 1000–2000, accompanied by frequency dependence, suggest that this oxide is a ferroelectric material like the hexagonal manganites $LnMnO_3$, i.e., the present system may be regarded as a multiferroic system. It is also characteristic that a broad peak appears around 260 K, a temperature which is close to the charge-ordering temperature of $Ho_{0.5}Ca_{0.5}MnO_3$ and $Er_{0.5}Ca_{0.5}MnO_3$ (Fig. 9). Since the electrical resistivity data excludes a possibility of long-range charge order in $Lu_{0.5}Ca_{0.5}MnO_3$, the behavior implies that there exists a short-range ordered phase below 260 K, such as a formation of small ferroelectric charge-ordered clusters, considering the discussion on the ferroelectricity owing to a charge ordering transition in a mixed-valence iron oxide $LuFe_2O_4$ [33]. The present curves taken with 10 and 100 kHz also show broad shoulders around 100 K, around which no anomaly was observed in both magnetic and resistivity measurements (Fig. 9). These phenomena, the peak around 260 K and the shoulder around 100 K, were qualitatively analogous to those of the charge-ordered oxide $Ho_{0.5}Ca_{0.5}MnO_3$. Further experimental studies are currently in progress to reveal the origins of these physical properties, and the results will be published in the near future.

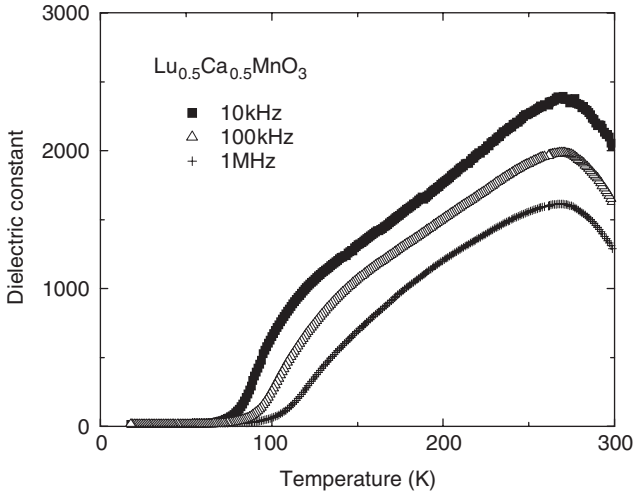

Fig. 10. Dielectric constant plotted against temperature, measured with the AC frequencies of 10, 100 kHz and 1 MHz for $Lu_{0.5}Ca_{0.5}MnO_3$. The details of the measurement were noted in Ref. [33].

4. Summary

It was found that the manganese perovskite oxides $Ln_{0.5}Ca_{0.5}MnO_3$ (*Ln* = Ho, Er, Tm, Yb and Lu) have an orthorhombic structure (space group *Pnma*). The Mn–O–Mn angles were calculated to be ~148–150°, revealing a very strained crystal structure in these oxides. Electrical resistivity measurements indicated both an insulating nature and a small magnetoresistance effect. DC magnetization measurements showed the three characteristic temperatures, which can be assigned to charge-order, antiferromagnetism of Mn moments, and possible glassy states. All of these temperatures were decreased for the heavier *Ln* ions, which is explained in connection with a difference of ionic radii of Ln^{3+} and Ca^{2+}, and a lowering of electron transfer. The charge-ordering transition was not clearly observed only for $Lu_{0.5}Ca_{0.5}MnO_3$ containing the smallest lanthanide ion, plausibly due to a large randomness of magnetic interactions arising from the ionic radii difference of Lu^{3+} and Ca^{2+}. In addition, preliminary measurements of AC dielectric response suggested that these manganites belong to a so-called multiferroic system.

References

[1] J.B. Goodenough, J.M. Longo, Landolt–Bornstein, Group III, vol. 4. Magnetic and Other Properties of Oxides and Related Compounds, Springer, New York, 1970, p. 126.
[2] S. Nomura, Landolt–Bornstein, Group III, vol. 12. Magnetic and Other Properties of Oxides and Related Compounds, Springer, New York, 1978, p. 368.
[3] H.L. Yakel, W.C. Koehler, E.F. Bertaut, E.F. Forrat, Acta Cryst. 16 (1963) 957.
[4] M. Bieringer, J.E. Greedan, J. Solid State Chem. 143 (1999) 132.
[5] A. Muñoz, J.A. Alonso, M.J. Martínez-Lope, M.T. Casáis, J.L. Martínez, M.T. Fernández-Díaz, Phys. Rev. B 62 (2000) 9498.
[6] D.G. Tomuta, S. Ramakrishnan, G.J. Nieuwenhuys, J.A. Mydosh, J. Phys.: Condens. Matter 13 (2001) 4543.
[7] T. Katsufuji, S. Mori, M. Masaki, Y. Moritomo, N. Yamamoto, H. Takagi, Phys. Rev. B 64 (2001) 104419.
[8] H. Sugie, N. Iwata, K. Kohn, J. Phys. Soc. Jpn. 71 (2002) 1558.
[9] K. Yoshii, H. Abe, J. Solid State Chem. 165 (2002) 131.
[10] For example, T. Lottermoser, T. Lonkai, U. Amann, D. Hohlwein, J. Ihringer, M. Fiebig, Nature 430 (2000) 541.
[11] See for example, Y. Tokura (Ed.), Colossal Magnetoresistive Oxides, Gordon & Breach, New York, 2000.
[12] J.B. Goodenough, Z.-S. Zhou, F. Rivadulla, E. Winkler, J. Solid State Chem. 175 (2003) 116 and references therein.
[13] P.G. Radaelli, D.E. Cox, M. Marezio, S.-W. Cheong, Phys. Rev. B 55 (1997) 3015.

[14] P.M. Woodward, T. Vogt, D.E. Cox, A. Aruraj, C.N.R. Rao, P. Karen, A.K. Cheetham, Chem. Mater. 10 (1998) 3652.
[15] C. Autret, C. Martin, A. Maignan, M. Hervieu, B. Raveau, G. Andre, F. Bouree, J. Solid State Chem. 165 (2002) 65.
[16] J. Blasco, J. Garcia, J.M. de Teresa, M.R. Ibarra, J. Perez, P.A. Algarabel, C. Marquina, C. Ritter, J. Phys.: Condens. Matter 9 (1997) 10321.
[17] T. Terai, T. Sasaki, T. Kakeshita, T. Fukuda, T. Saburi, H. Kitagawa, K. Kindo, M. Honda, Phys. Rev. B 61 (2000) 3488.
[18] J. Lopez, O.F. de Lima, P.N. Lisboa-Filho, F.M. Araujo-Moreira, Phys. Rev. B 66 (2002) 214402.
[19] A. Arulraj, R. Gundakaram, A. Biswas, N. Gayathri, A.K. Raychaudhuri, C.N.R. Rao, J. Phys.: Condens. Matter 10 (1998) 4447.
[20] A. Arulraj, P.N. Santhosh, R.S. Gopalan, A. Guha, A.K. Raychaudhuri, N. Kumar, C.N.R. Rao, J. Phys.: Condens. Matter 10 (1998) 8497.
[21] B. Garcia-Landa, J.M. de Teresa, M.R. Ibarra, C. Ritter, R. Drost, M.R. Lees, J. Appl. Phys. 83 (1998) 7664.
[22] A. Sundaresen, P.L. Paulose, R. Mallik, E.V. Sampathkumaran, Phys. Rev. B 57 (1998) 2690.
[23] C. Martin, A. Maignan, M. Hervieu, B. Raveau, Phys. Rev. B 60 (1999) 12191.
[24] A. Maignan, C. Martin, G. Van Tendeloo, M. Hervieu, B. Raveau, Phys. Rev. B 60 (1999) 15214.
[25] W. Song, F. Luo, Y.H. Huang, C.H. Yan, B.Z. Sun, L.L. He, J. Appl. Phys. 96 (2004) 2731.
[26] F. Izumi, T. Ikeda, Mater. Sci. Forum 321–324 (2000) 198.
[27] R.D. Shannon, Acta Cryst. A 32 (1976) 751.
[28] L.M. Rodriguez-Martinez, J.P. Attfield, Phys. Rev. B 54 (1996) R15622.
[29] F. Damay, C. Martin, A. Maignan, B. Raveau, J. Appl. Phys. 82 (1997) 6181.
[30] J.H. Van Vleck, The Theory of Electric and Magnetic Susceptibilities, Oxford University Press, Oxford, 1965.
[31] See for example, J.A. Mydosh, Spin Glasses, Taylor & Francis, London, 1993.
[32] S. Yunoki, T. Hotta, E. Dagotto, Phys. Rev. Lett. 84 (2000) 3714.
[33] N. Ikeda, H. Ohsumi, K. Ohwada, K. Ishii, T. Inami, Y. Murakami, K. Kakurai, K. Yoshii, M. Mori, Y. Horibe, H. Kito, Nature 436 (2005) 1136 and references therein.